RESEARCH PAPER

Quantitative evaluation of geological uncertainty and its influence on tunnel structural performance using improved coupled Markov chain

Jin-Zhang Zhang[1,2] · Hong-Wei Huang[1] · Dong-Ming Zhang[1] · Kok Kwang Phoon[2,3] · Zhong-Qiang Liu[4] · Chong Tang[2]

Abstract

The geo-structures embedded in the multiple variable strata could be significantly affected by the geological uncertainty. The quantitative evaluation of geological uncertainty and its influence on the structural safety of embedded tunnels are seldom studied in the past. This paper aims to analyse the effect of geological uncertainty on the structural performance of tunnel using the proposed stochastic geological modelling framework. The geological uncertainty is characterized using an improved coupled Markov chain model based on sparse limited boreholes. A mapping approach is presented to solve the mesh asymmetry problem between the simulated strata and the numerical tunnel model. The tunnel structural performance analysis is then conducted based on the combined model considering the geological uncertainty and tunnel structure. A geological uncertainty index (GUI) is proposed to quantitatively evaluate the level of uncertainty of each borehole and the whole site. The effect of the borehole layout scheme on uncertainty evaluation of factor of safety of tunnel structure is investigated by a large number of stratigraphic realizations. Boreholes collected from Norway with relatively more considerable variability and from Shanghai with relatively more minor variability are adopted as case studies to illustrate the proposed probabilistic analysis framework. The results show that the boreholes with larger GUI values and closer to tunnel locations have a greater weight to affect the embedded tunnel structural performance in uncertain geological strata.

Keywords Coupled Markov chain · Geotechnical uncertainty · Stochastic geological framework · Tunnel performance · Uncertainty quantification

✉ Dong-Ming Zhang
09zhang@tongji.edu.cn

1 Key Laboratory of Geotechnical and Underground Engineering of Minister of Education and Department of Geotechnical Engineering, Tongji University, Shanghai 200092, China

2 Department of Civil and Environmental Engineering, National University of Singapore, Singapore 117576, Singapore

3 Singapore University of Technology and Design, Singapore 487372, Singapore

4 Department of Natural Hazards, Norwegian Geotechnical Institute (NGI), Sognsveien 72, 0855 Oslo, Norway

1 Introduction

With the rapid development of urbanization, metro tunnels are being largely constructed and operated in recent years. The structural safety of the tunnel has always been one of the most concerned issues of the governor and engineers [16, 18, 45, 49]. Once the tunnel accident occurs, it will cause enormous casualties, economic losses and social severe adverse effects. Meanwhile, the embedded environment of geo-structures is complex and uncertain [38, 46]. The uncertainty can be mainly divided into two categories [10]: spatial variability of soil properties within one nominally homogeneous layer [21, 26] and geological uncertainty in heterogeneous layer [8, 34]. In past decades, much attention has been attracted to analyse the influence of spatial variability of soil properties on the performance of geotechnical systems such as tunnels

[3, 11, 20, 31, 32, 47, 48]. On the other hand, geological uncertainty also exists in reality and plays a significant role in geo-structure performance [10, 14, 25]. Due to the limitation of geotechnical investigation techniques and project budgets, only a limited number of boreholes can be afforded in a practical project [12]. Thus, the geological information can be accurately known at only some spare location of boreholes. The subsurface geological information at other locations is difficult to obtain in advance [40]. Without accurate stratum information, accidents are prone to occur during the construction process. The accident at Pinheiros Station on the new line 4 of the São Paulo Metro caused seven casualties. The subway line did not start operating until nearly 2 years later due to unforeseen geological conditions [30]. Therefore, how to characterize the geological uncertainty and its effect on geo-structures is still a challenge to geologists and engineers.

Some efforts have been devoted to the characterization of geological uncertainty and its influence [23, 40]. There are two groups to model the geological uncertainty. The first group is the variogram simulation method based on geostatistics [6], such as the Kriging approach [4], Gaussian threshold model [27] and multi-point geostatistical approach [35]. However, these methods strongly rely on the quality and adequate borehole data for site-specific projects. The second choice to characterize the geological uncertainty is Markov model, including Markov random field model [5, 39] and Markov chain model [2]. Stochastic geological modelling based on Markov random field theory was proposed [25, 37, 42] to simulate the geological uncertainty. This method has been applied to assess the effect on slope stability [12, 41] and tunnels [40]. However, the orientation of the stratum needs to know in advance for this method [1, 24]. Coupled Markov chain (CMC) is another effective model to simulated geological uncertainty proposed by Elfeki and Dekking [8]. Qi et al. [34] proposed a practical method to estimate the horizontal transition probability matrix (HTPM) and has been applied to a slope problem [7, 23]. Due to the limitation of the crucial hypothesis for determining HTPM, an improved coupled Markov chain method was proposed. Based on this method, this paper applies the improved CMC model to evaluate the structural performance of the tunnel in the presence of geological uncertainty using borehole data. In the variable and uncertain stratum, the performance of tunnel's structure will have a larger difference with the homogeneous formation [40]. The horizontal tunnel convergence (ΔD_h) and bending moment are the two critical indexes of the tunnel's structural performance, according to the relevant literature [13, 44]. Thus, it is necessary to incorporate geological uncertainties in the tunnel probabilistic analysis framework to reveal the uncertainty in the factor of safety

of ultimate limit states of segment strength (ULS) and serviceability limit state (SLS).

The geological uncertainty of different sites is also different due to the complex geological, environmental and physical–chemical processes [33]. How to quantitatively evaluate the level of geological uncertainty is also a problem to be solved. Thus, this paper aims to study the influence of geological uncertainty on the tunnel and quantitatively evaluate the level of geological uncertainty. A probabilistic analysis framework was proposed, which combines the simulation of geological uncertainty using the improved CMC model and the simulated tunnel using the finite difference method (FDM) model. This paper is organized in the following manner. Firstly, the improved CMC approach is adopted for characterizing the geological uncertainty and the presented probabilistic analysis framework is briefly reviewed. Secondly, a geological uncertainty index is proposed to evaluate each borehole's level of geological uncertainty and the whole site. Next, Norway and Shanghai sites are used as two case studies to explore the effect of geological uncertainty on the performance of tunnel structures under the different levels of geological uncertainty. Finally, the concluding remarks are presented. This work has the potential contribution to help the engineers pay more attention to the borehole with larger weight to affect the tunnel structural safety in geological uncertainty.

2 Geological uncertainty modelling framework

As illustrated in Fig. 1, the proposed probabilistic analysis framework is involved two major steps: improved CMC model and map the simulated strata into FDM model. The improved CMC model is employed to simulate the geological uncertainty. By combining the simulated uncertain strata with the finite difference analysis method, a probabilistic analysis can be achieved to monitor the response of tunnel structural performance. The detailed explanation of the improved CMC model and mapping method is introduced in Sects. 2.1 and 2.2.

2.1 Improved coupled Markov chain model

Coupled Markov chain model has the ability to characterize the heterogeneity of geological formations [8]. It is easy to explain, has few parameters and has high applicability [9]. The two-dimensional CMC model is more suitable to simulate the geological uncertainty than the one-dimensional CMC model, which can only characterize one direction. As shown in Fig. 2, the domain is divided into $Nx \times Ny$ cells of the same size, and each cell corresponds
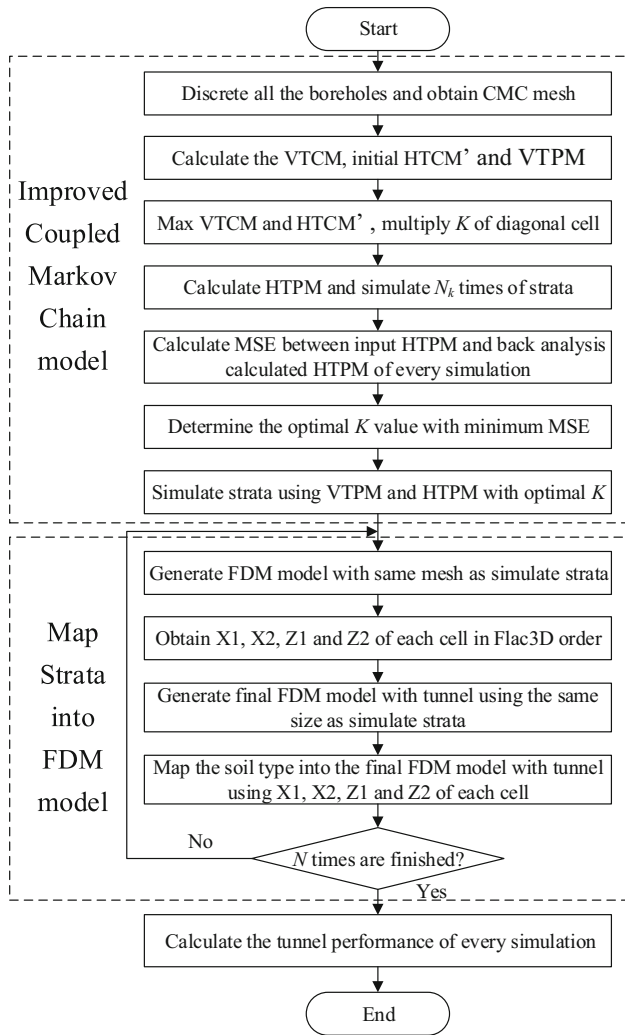
Fig. 1 Framework of tunnel probabilistic analysis considering geological uncertainty
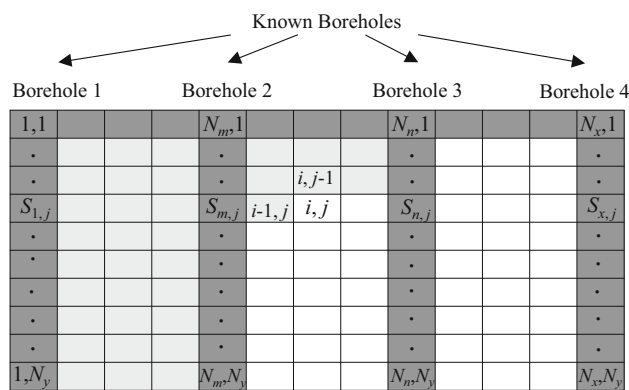

Fig. 2 Schematic of using coupled Markov chain to simulate two-dimensional domain

to its state. The basic idea of the CMC model is that the state of the current step depends only on the state in the previous step. This means that the state X_{ij} of the cell (i, j)

depends on states $X_{i-1, j}$ and $X_{i, j-1}$ of the cells on the left $(i - 1, j)$ and on the top $(i, j - 1)$ of the current cell in the domain. For simplicity, let the state of cells (i, j), $(i - 1, j)$, $(i, j - 1)$ and (N_x, j) is S_k, S_l, S_m and S_q, respectively. The conditioning formula can be expressed by

$$
\begin{aligned}
P_{lm,k|q} &= P(X_{i,j} = S_k | X_{i-1,j} = S_l, X_{i,j-1} = S_m, X_{N_x,j} = S_q) \\
&= \frac{p_{lk}^h \cdot p_{kq}^{h(N_x-i)} \cdot p_{mk}^v}{\sum_{f=1}^n p_{lf}^h \cdot p_{fq}^{h(N_x-i)} \cdot p_{mf}^v}
\end{aligned}
\tag{1}
$$

where $p_{kq}^{h(N_x-i)}$ is the $(N_x - i)$-step horizontal transition probability from S_k to S_q and p_{mk}^v is the vertical transition probability from S_m to S_k.

The vertical and horizontal transition probability matrices (VTPM and HTPM) are the two significant parameters to simulate geological uncertainty. They can be easily calculated through the transition count matrix. Taking the calculated process of VTPM of three soil types as an example, the vertical transition count matrix (T^v) can be obtained by counting the number of transfers of different soil types, as shown in Eq. (2). For example, the transition probability p_{ij}^v in VTPM can be calculated by Eq. (3).

$$
T^v = \begin{pmatrix} T_{11}^v & T_{12}^v & T_{13}^v \\ T_{21}^v & T_{22}^v & T_{23}^v \\ T_{31}^v & T_{32}^v & T_{33}^v \end{pmatrix}
\tag{2}
$$

$$
p_{ij}^v = \frac{T_{ij}^v}{\sum_{n=1}^u T_{in}^v}
\tag{3}
$$

where p_{ij}^v is defined as the ratio of the number of transitions from soil type i to soil type j with the number of transitions from soil type i to all states ($u = 3$ in this example). The HTPM is challenging to determine due to the limited boreholes in the horizontal direction [23]. There are two main limitations of determining the HTPM for the current method proposed by Qi et al. [34]. The first is the strict assumption that HTPM is entirely determined by VTPM and the ratio of horizontal length to vertical length (K). Another shortcoming is that the borehole data are not fully used in the process of determining K value, resulting in greater uncertainty. The main contribution of the improved CMC model is to enhance the rationality of HTPM estimation based on limited borehole data. The main steps of this improved CMC method are summarized below.

$$
T^h = \begin{pmatrix} KT_{11}^{hv} & T_{12}^{hv} & T_{13}^{hv} \\ T_{21}^{hv} & KT_{22}^{hv} & T_{23}^{hv} \\ T_{31}^{hv} & T_{32}^{hv} & KT_{33}^{hv} \end{pmatrix}
\tag{4}
$$

As plotted in Fig. 1, the first step is to calculate the vertical transition count matrix (VTCM) and initial

horizontal transition count matrix (HTCM'). The VTCM (T^v) can be easily counted and is shown in Eq. (2). For example, T^v_{11} means the number of transitions from state 1 to state 1 in the vertical direction. Following the same process, the HTCM' ($T^{h'}$) can also be obtained, then taking the larger value of VTCM and HTCM' in the corresponding position to get the intermediate matrix (e.g. T^{hv}_{11}). Meanwhile, the final horizontal transition count matrix can be obtained by multiplying the diagonal elements of the intermediate matrix by K value based on Walther's law, as shown in Eq. (4). Thus, VTPM and HTPM of the CMC input parameters can be obtained, which is defined as the ratio of the number of transitions from state S_l to state S_k with the number of transitions from state S_l to all states (e.g. $p^v_{11} = T^v_{11}/(T^v_{11} + T^v_{12} + T^v_{13})$). The third step is to determine the K value. Assuming N_k different K values, N times of Monte Carlo simulations are performed for each K value. The evaluation index is the mean square error (MSE) of the error matrix for input HTPM and back analysis calculated HTPM. The optimal result is the K value with the minimum MSE of the error matrix. The final step is to simulate the geological uncertainty using the VTPM and HTPM calculated using the optimal K value.

2.2 Map the simulated strata into FDM tunnel model

In this section, a mapping approach is presented to solve the mesh asymmetry problem between the simulated stratum and the numerical FDM tunnel model. A common challenge is that the mesh of the FDM model and simulated uncertain strata generally cannot be precisely the same. In this study, the FDM model has a tunnel, so the mesh near the tunnel must be irregular which is typical in geotechnical engineering numerical analysis. Generally, the size of every cell of simulated formation is regular and consistent. Therefore, this difficulty can be solved in two steps. Firstly, the four boundaries of each cell of the simulated formation using the CMC model can be obtained. Meanwhile, the corresponding type of geotechnical properties is also given. Secondly, using the four boundaries and the soil type of each cell in simulated strata to redefine the type of geotechnical properties of each mesh in the FDM model. It is worth noting that the mesh size (i.e. height and width) of the FDM model should be as close as possible to the cells of the simulated uncertain formation. There are two basic rules of the mapping process. The first one is that if the area of the simulated strata cell is greater than half of the area of the corresponding zone in the numerical model area, the mapping will be performed. Therefore, the mesh size in the numerical model must be less than twice the size of the simulated formation cell. Otherwise, the mapping will not

be performed because a zone in the FDM model cannot have two soil types. The second rule is that if the zone in the numerical model is mapped twice, the soil type in the second mapping will cover the soil type in the front.

The mapping process of simulated formation into the numerical model is shown in Fig. 3. Figure 3a shows the simulated formation with four soil states (state 1–4) represented by yellow, purple, grey and green. If the mesh size in the numerical model is 1, 1/2, 1/3, 1/4 … 1/n times than the size of the simulated formation cell, the mapping result will be perfect, as shown in Fig. 3a, b. In FLAC. 3D software, the number of the zones is from left to right and from bottom to top, as shown in Fig. 3c (Zone 1–6). Taking it as an example, the mapping process is as follows. Step 1: zone 1 and 3 are mapped in yellow; step 2: zone 2 and 4 are mapped in pink; step 3: zone 3 and 5 are mapped in grey; and step 4: zone 4 and 6 are mapped in green. It can be seen that zone 3 and 4 are covered by the second mapping. The process is followed by the second mapping rule, as introduced above. In Fig. 3d, the mesh size in the numerical model is exactly twice the size of the simulated formation cell. The size of cell in simulated strata has just reached 50% of the numerical model zone. Zone 1 and zone 2 are firstly mapped into yellow and pink and then coved by grey and green.

3 Quantitative evaluation of the geological uncertainty

To quantitatively investigate the level of the geological uncertainty, a geological uncertainty index (GUI) is proposed as:

$$\text{GUI} = \frac{1}{k} \sum_{i=1}^{k} \sum_{j=1}^{d} \frac{N_{k(V_{(j)} \neq S_{(j)})}}{d} \tag{5}$$

where k is the number of boreholes except the two boreholes at the left and right boundary; d is the number of cells in the depth or vertical direction; V and S mean the virtual
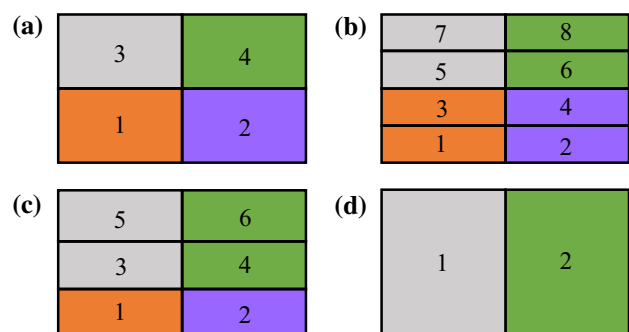

Fig. 3 Mapping process of simulated formation into the numerical model

strata and simulated strata for comparison; and $N_{k(V(j) \neq S(j))}$ is the totally different number of cells for kth borehole between the simulated strata (as shown in Fig. 4a) and virtual strata (as shown in Fig. 4b). For a specific site, the simulated strata are chosen as the most likely realization for all collected boreholes using the improved CMC model. The most likely realization means that the soil type of each cell is selected as the most frequently occurs in the Monte Carlo simulations. It can be considered the most likely geological profile based on the measured borehole data. The virtual strata can be obtained using a straight line to connect the corresponding soil layer revealed by the two boreholes on the left and right sides. This GUI value calculated using Eq. (5) reflects the average level of geological uncertainty for the whole site. Meanwhile, the uncertainty level of each borehole can also be calculated using the proposed formula; only need to count the number of different cells in the selected borehole. A larger GUI value means greater uncertainty in this field, so more boreholes are needed to reduce the uncertainty. On the contrary, a smaller GUI value means fewer boreholes are enough to simulate the uncertain stratum. The proposed indicator GUI will be used to assess the geological uncertainty of collected boreholes from Norway and Shanghai sites. Meanwhile, the impact of borehole uncertainty on the response of the embedded tunnel performance in the uncertain formation will also be discussed in the case study section.

4 Case study of Norway site

4.1 Borehole data of Norway

The collected borehole data from a construction site of Norway are used to simulate the uncertain stratum, which is plotted in Fig. 5. It can be seen that the size of the domain is 70 × 30 m with eight boreholes. The soil layer within the collected boreholes can be classified into four types, i.e. topsoil, clay, quick clay and sand, which are
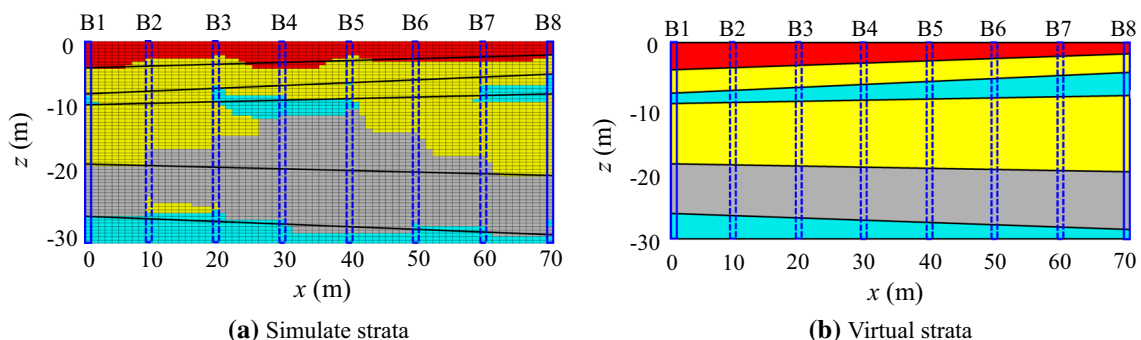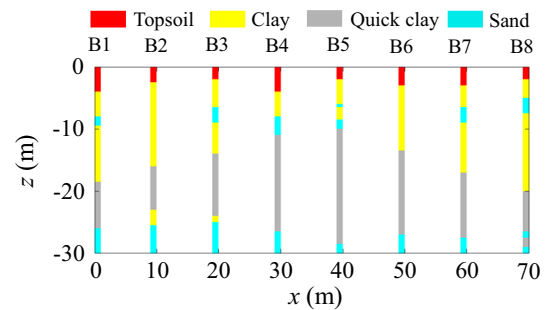

Fig. 5 Stratum information revealed by boreholes in Norway

coloured red, yellow, grey and cyan in Fig. 5. For clarity, the four soil types are represented by soil types 1 to 4. In this study, all the soil classification of borehole data is extracted from the site investigation report. The commonly used method to classify the different soil types is the general classification system [22]. It is useful for grouping together soils of similar particle size, water content, unit weight, colour, odour and plasticity characteristics. In addition, there are also some other methods, such as cone penetration test (CPT) classification, piezocone penetration test (CPTU) classification and dilatometer test (DMT) classification. The details about these methods can be found in the previous literature [22]. The boreholes need to discrete into cells firstly using the same interval. The proper size of the cell in the CMC model would be less or equal to the minimum thickness of the geological unit in the corresponding direction [8]. This can reasonably reproduce the geological features. In this case study, the sampling interval in horizontal and vertical is 1 and 0.5 m because the minimum thickness of the strata revealed by boreholes is 0.5 m at the B5 borehole, as shown in Fig. 5. The sampling interval in the horizontal direction is generally larger than the value in vertical due to the relatively large scale of soil transition variability in the horizontal direction than that in the vertical direction [34].

(a) Simulate strata

(b) Virtual strata

Fig. 4 Diagram of the proposed geological uncertainty index

4.2 Estimation of transition probability matrix

In this section, the collected Norway boreholes are used to illustrate the effect of the borehole layout scheme on soil transition simulation. The estimation of VTPM and HTPM is only based on the contained boreholes of each layout scheme. The eight different layout schemes are designed based on boreholes to reflect the effect of both borehole number and location. Following the introduction in Sect. 2.1, the estimated VTPM and HTPM of all eight boreholes, namely the BS8 borehole layout scheme, is shown in Table 1. The optimal K value of BS8 is 9.4, which is also given in Table 1. It can be as a basic result to compare with the calculated VTPMs and HTPMs from different layout schemes. All the designed borehole layout schemes must include the boreholes at the two outmost columns. In other words, boreholes B1 and B8 are included in all layout schemes.

Figure 6 presents the numerical model with tunnel using the most likely realization for all eight borehole layout schemes. It is worth mentioning that the depth of the domain has increased by 15 m to avoid the boundary effect of the model. As shown in Fig. 5, the length of boreholes is 30 m. The type of soil is all adopted as state 4 for the increased 15 m soil depth, as shown by the red dotted line in Fig. 6. This is reasonable because the revealed soil type of all boreholes at the depth of 30 m is soil state 4. It can be seen that the location of the additionally added 15 m soil layer is relatively far away from the tunnel. The aim of it is to avoid the boundary effect on tunnel structural performance. It is worth noting that this added soil layer is the same at all borehole layout schemes. The small black rectangle means the location of eight boreholes.
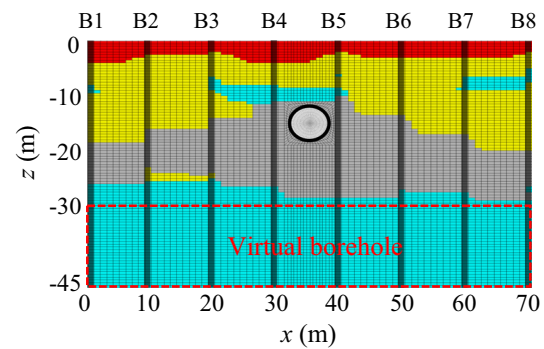

Fig. 6 Tunnel model and borehole locations for all boreholes (red: topsoil; yellow: clay; grey: quick clay; cyan: sand)

4.3 Effect of borehole layout scheme on strata simulation

The estimated VTPMs and HTPMs of other different borehole layout schemes are listed in Tables 2 and 3, respectively. The boreholes contained in each layout scheme are also shown in Table 2. Meanwhile, the optimal K value of each layout scheme for estimation HTPM is also presented in Table 3. The optimal K value basically decreases with the increase in the number of boreholes. The optimal K value can be roughly determined using a large spacing and then using a small spacing to accurately determine. This process of determining K value is fast and effective, especially for the smaller number of borehole schemes. It can be seen that the differences in the VTPMs (HTPMs) are affected not only by the number of boreholes but also the location, such as the BS4A and BS4B. These differences will cause the different CMC simulation results, leading to a different response of embedded tunnel structural performance.

Figure 7 shows the most likely realizations for eight different borehole layout schemes using the improved CMC model. They are used to present the effect of borehole layout schemes on the simulation of formation. The CMC realizations for each layout scheme are simulated using the corresponding conditional boreholes, VTPMs and HTPMs. Meanwhile, the shown realizations have mapped the simulated strata into the numerical tunnel model. In these realizations, the domain of the CMC model is a rectangular area with an x, z range of [0 m, 70 m] and [0 m, 30 m], respectively. Similarly, the depth in vertical direction has also increased by 15–45 m for every borehole layout scheme to avoid the boundary effect.

The Monte Carlo (MC) simulations are used to address the probabilistic tunnel analysis under the different borehole layout schemes. Figure 8 shows the influence of the number of simulations on the mean value and coefficient of variance (COV) of tunnel safety factor ($0.4\%D/\Delta D_h$). It can be seen that both the variation of mean and COV are

Table 1 VTPM and HTPM for all eight boreholes

State	1	2	3	4
(a) VTPM for BS8				
1	0.822	0.178	0.000	0.000
2	0.000	0.914	0.034	0.052
3	0.000	0.011	0.950	0.039
4	0.000	0.069	0.042	0.889
(b) HTPM for BS8 [K = 9.4]				
1	0.972	0.028	0.000	0.000
2	0.004	0.971	0.012	0.012
3	0.000	0.015	0.981	0.004
4	0.000	0.022	0.021	0.957

Table 2 VTPMs for various borehole layout schemes

State	1	2	3	4	State	1	2	3	4
(a) BS3A [boreholes (1,3,8)]					*(b) BS3B [boreholes (1,5,8)]*				
1	0.813	0.188	0.000	0.000	1	0.813	0.188	0.000	0.000
2	0.000	0.910	0.039	0.051	2	0.000	0.913	0.029	0.058
3	0.000	0.020	0.922	0.059	3	0.000	0.000	0.941	0.059
4	0.000	0.094	0.031	0.875	4	0.000	0.125	0.083	0.792
(c) BS4A [boreholes (1,3,5,8)]					*(d) BS4B [boreholes (1,4,6,8)]*				
1	0.800	0.200	0.000	0.000	1	0.846	0.154	0.000	0.000
2	0.000	0.900	0.033	0.067	2	0.000	0.930	0.035	0.035
3	0.000	0.011	0.943	0.046	3	0.000	0.000	0.944	0.056
4	0.000	0.105	0.053	0.842	4	0.000	0.057	0.057	0.886
(e) BS5A [boreholes (1,2,4,6,8)]					*(f) BS5B [boreholes (1,3,5,7,8)]*				
1	0.839	0.161	0.000	0.000	1	0.808	0.192	0.000	0.000
2	0.000	0.932	0.034	0.034	2	0.000	0.903	0.035	0.062
3	0.000	0.010	0.942	0.049	3	0.000	0.009	0.945	0.046
4	0.000	0.047	0.047	0.907	4	0.000	0.106	0.043	0.851
(g) BS6 [boreholes (1,2,3,5,7,8)]					*(h) BS7 [boreholes (1,2,3,4,5,6,8)]*				
1	0.807	0.194	0.000	0.000	1	0.821	0.180	0.000	0.000
2	0.000	0.910	0.035	0.055	2	0.000	0.914	0.033	0.053
3	0.000	0.016	0.943	0.041	3	0.000	0.013	0.950	0.038
4	0.000	0.091	0.036	0.873	4	0.000	0.064	0.048	0.889

Table 3 Optimal K value and HTPMs for various borehole layout schemes

| State	1	2	3	4	State	1	2	3	4
(a) BS3A [boreholes (1,3,8), K = 24.8]					*(b) BS3B [boreholes (1,5,8), K = 25.6]*				
1	0.988	0.012	0.000	0.000	1	0.985	0.015	0.000	0.000
2	0.000	0.986	0.010	0.004	2	0.000	0.979	0.014	0.007
3	0.000	0.012	0.986	0.002	3	0.000	0.016	0.982	0.003
4	0.000	0.008	0.012	0.980	4	0.000	0.015	0.015	0.971
(c) BS4A [boreholes (1,3,5,8), K = 16.8]					*(d) BS4B [boreholes (1,4,6,8), K = 17.9]*				
1	0.990	0.010	0.000	0.000	1	0.981	0.019	0.000	0.000
2	0.000	0.984	0.010	0.006	2	0.002	0.979	0.013	0.007
3	0.000	0.012	0.985	0.003	3	0.000	0.016	0.980	0.004
4	0.000	0.011	0.009	0.981	4	0.000	0.016	0.011	0.974
(e) BS5A [boreholes (1,2,4,6,8), K = 14.2]					*(f) BS5B [boreholes (1,3,5,7,8), K = 17.1]*				
1	0.981	0.019	0.000	0.000	1	0.984	0.016	0.000	0.000
2	0.002	0.979	0.013	0.007	2	0.001	0.981	0.011	0.007
3	0.000	0.016	0.980	0.004	3	0.000	0.012	0.984	0.003
4	0.000	0.016	0.011	0.974	4	0.000	0.016	0.014	0.970
(g) BS6 [boreholes (1,2,3,5,7,8), K = 13.1]					*(h) BS7 [boreholes (1,2,3,4,5,6,8), K = 10.2]*				
1	0.982	0.018	0.000	0.000	1	0.970	0.030	0.000	0.000
2	0.001	0.978	0.012	0.009	2	0.004	0.972	0.013	0.011
3	0.000	0.016	0.981	0.003	3	0.000	0.016	0.980	0.004
4	0.000	0.020	0.015	0.965	4	0.000	0.019	0.020	0.961
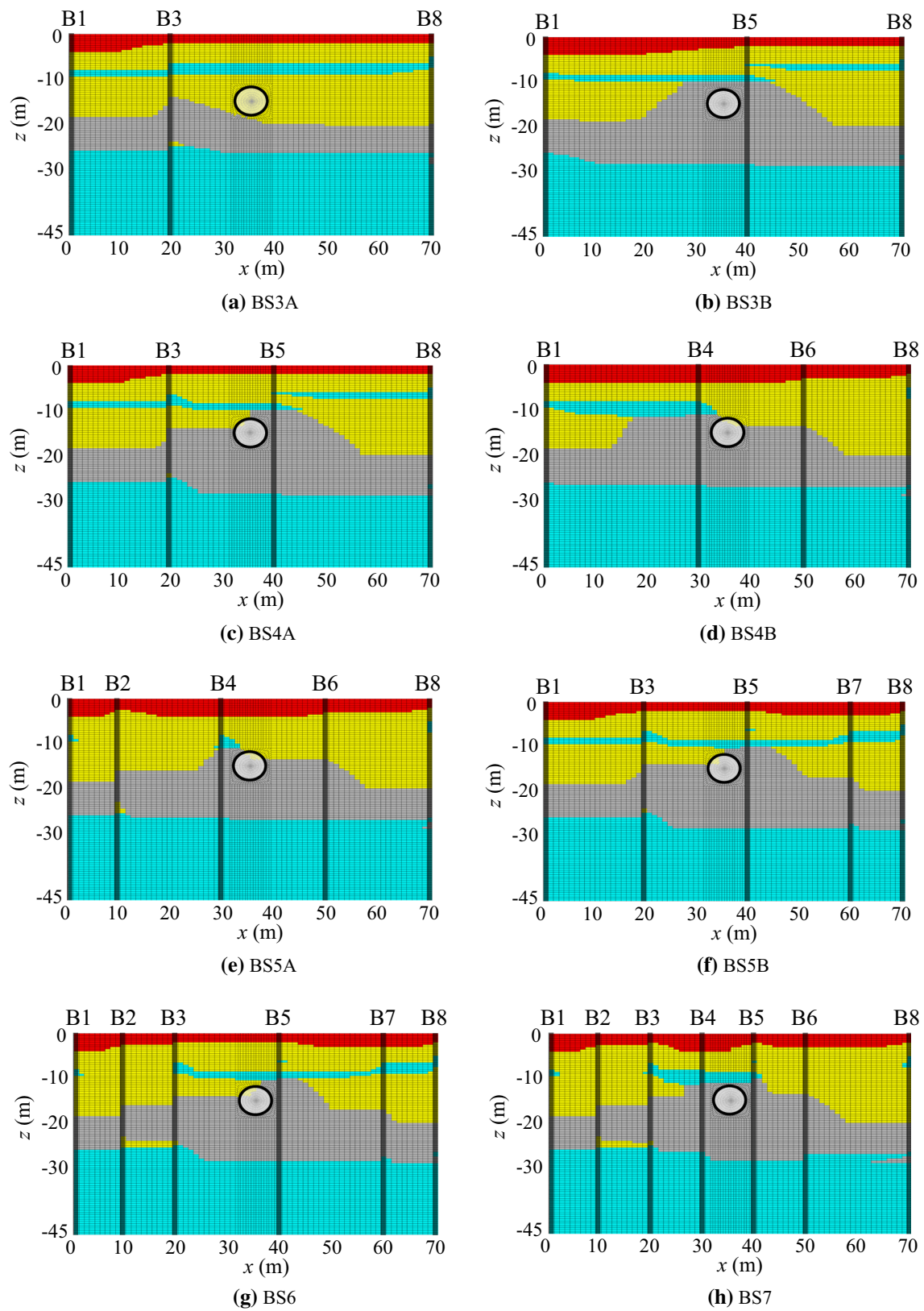
Fig. 7 Most likely realizations for different borehole schemes with tunnel model (red: topsoil; yellow: clay; grey: quick clay; cyan: sand)
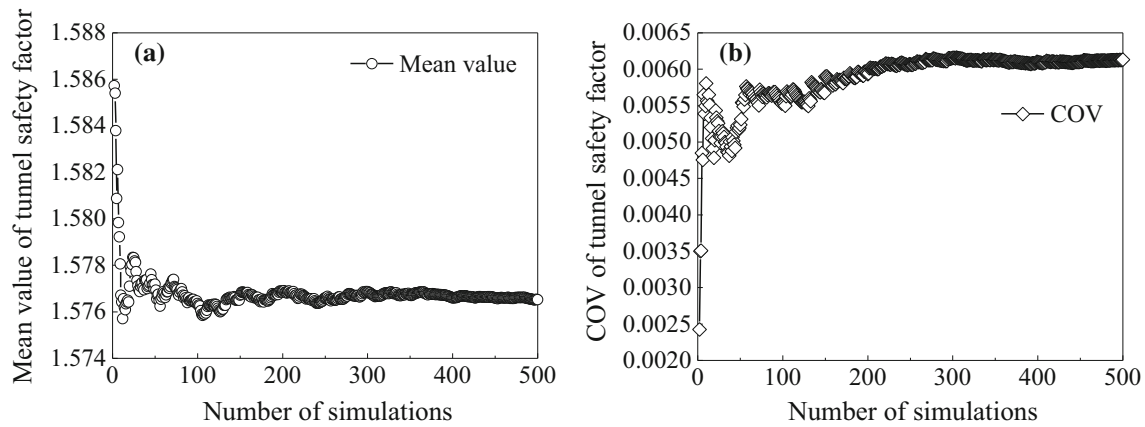
Fig. 8 Effect of number of simulations on mean value and COV of tunnel safety factor

converged when the MC simulation runs is set to 500. The centre line of the tunnel in vertical and horizontal direction is located at − 15 m and 35 m for all layout schemes. A tunnel embedded into this geological uncertainty strata with its outer diameter $D = 6.2$ m and lining thickness $t = 0.35$ m is considered. The elastic modulus and Poisson's ratio of the tunnel are set at 34.5 GPa and 0.2. Meanwhile, the effective rigidity ratios of the tunnel lining are set to 0.67 to consider the effect of the segment joints on the rigidity of the tunnel lining [15]. The drained condition is assumed for the soil to focus on the long-term structural performance of tunnel lining. A set of soil parameters including Young's modulus (E), Poisson's ratio (v), effective cohesion (c'), effective friction angle (φ') and unit weight (γ) for all soil types are summarized in Table 4. The Mohr–Coulomb model is adopted as a constitute model of soil which is most widely used in geotechnical engineering [17, 29]. The unassociated flow rule is used in the Mohr–Coulomb failure criterion of FLAC 3D software [19].

4.4 Evaluation of borehole uncertainty of Norway site

Table 5 presents the GUI value of each borehole and the average level of the site for the collected Norway case using the proposed quantitatively evaluating approach

Table 4 Parameters for various types of soil for tunnel structural performance analysis

| Soil types	E (MPa)	v	c' (kPa)	φ' (°)	γ (kN/m^3)
State 1	10	0.35	0	22	1800
State 2	30	0.33	6	28.5	1850
State 3	12	0.4	18	14	1850
State 4	40	0.3	0	35	1850

introduced in Sect. 3. Note that the simulated strata to calculate the GUI value are the most likely realization using all eight collected boreholes. In this case, the length of boreholes is 30 m which is discretized with 0.5-m intervals, resulting in 60 cells in the vertical direction. Thus, the d value in Eq. (5) is equal to 60. The different number of cells can be obtained by comparing the simulated strata and virtual strata in the location of selected boreholes, as shown in Fig. 4. Then, the GUI value of each borehole and whole site can be calculated, as given in Table 5. The average GUI value represents the average level of geological uncertainty of this site. The average GUI value is 34.2% for the collected Norway site, indicating the level of geological uncertainty is relatively larger. It can be seen that the GUI value of borehole B4 and B5 even reaches 45%. Meanwhile, the location of these two boreholes is near the tunnel. Therefore, it is foreseeable that these two boreholes will play a significant role in the borehole layout scheme. The results of the tunnel structural performance under different borehole layout schemes are discussed in the following.

4.5 Assessment of the performance of tunnel

Figure 9 presents the mean value and COV of horizontal tunnel convergence (ΔD_h) for different borehole schemes. The horizontal tunnel convergence is a mostly concerned indicator by engineers [16, 36]. As shown in Fig. 9a, the "real" ΔD_h means the calculated ΔD_h for the most likely realization of CMC simulation for eight boreholes, plotted in Fig. 7. This result $\Delta D_h = 15.759$ mm will be the "real" result to compare with the calculated result of different layout schemes. The relative error (RE) can be defined as ("real" ΔD_h – calculated ΔD_h)/"real" ΔD_h. In total, the mean value of ΔD_h is closer to the "real" ΔD_h with the increase in the number of boreholes, especially for the BS6 and BS7 with a much smaller RE value. It is worth noting

Table 5 Geological uncertainty index for Norway case

Borehole	B2	B3	B4	B5	B6	B7	Average
Different cells	16	18	27	27	20	15	20.5
GUI	26.7%	30%	45%	45%	33.3%	25%	34.2%
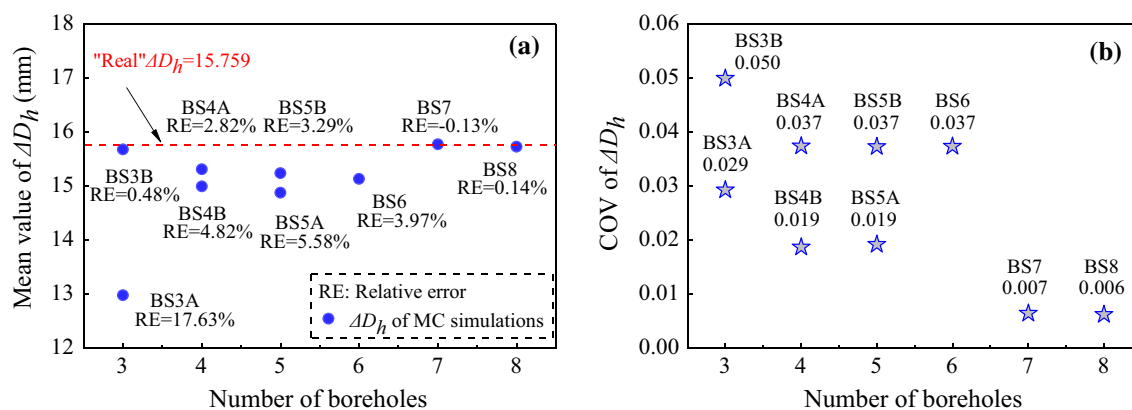
Fig. 9 Mean value and COV of ΔD_h for different borehole schemes

that the RE value is only 0.48% at the BS3B *[boreholes (1,5,8)]*. The RE value of BS3A *[boreholes (1,3,8)]* with three boreholes is as high as 17.63%, indicating that boreholes' location is also crucial for simulating the geological uncertainty. As shown in Table 5, the GUI value of borehole B5 is 45% which is larger than the value of B3 (30%). Meanwhile, the location of borehole B5 is more near to the location of the tunnel than B3. Therefore, borehole B5 has a more significant weight on the structural performance response of the tunnel in this uncertain stratum compared with borehole B3.

Figure 9b shows the COV of ΔD_h for different layout schemes. Compared with Fig. 9a, b, it is interesting that the performance of BS4A and BS4B is very similar to BS5A and BS5B borehole layout schemes. For example, the RE value of borehole layout scheme BS4B *[boreholes (1,4,6,8)]* and BS5A *[boreholes (1,2,4,6,8)]* is 4.82% and 5.58%, respectively. The COV of ΔD_h for these two layout schemes is the same as 0.019. The addition of borehole B2 did not contribute much to reducing uncertainty in the BS5A layout scheme. Thus, in the case of limited project budgets, the borehole B2 can be relatively abandoned first. It also means that the weight of each borehole is different. The GUI value of borehole B2, B4 and B6 is 26.7%, 45% and 33.3%, respectively. The boreholes B4 and B6 are located on both sides of the tunnel, while B2 and B4 are located on the same side of the tunnel. Meanwhile, borehole B2 is far away from the location of the tunnel. Thus, the contribution of borehole B2 is little in the BS5A borehole layout scheme.

For the structure embedded underground, the performance of the tunnel concerning the ultimate limit states of segment strength (ULS) and serviceability limit state (SLS) is the primary concern in the design of a tunnel [13, 43]. Therefore, the two factors of safety (FS) can be obtained. In this paper, the plastic theory is used to evaluate the safety of the tunnel segment structure based on the ultimate limit state of reinforced concrete [43]. It can be considered that the tunnel structure is failure when the combination of internal forces (M, N) exceeds the corresponding limit state (M_{Lm}, N_{Lm}) on the ultimate bearing envelope of the tunnel segment, and the detailed introduction can be found in the previous literature [13]. Thus, the F_{S1} is defined as:

$$F_{S1} = \frac{\sqrt{N_{Lm}^2 + M_{Lm}^2}}{\sqrt{N^2 + M^2}} \quad (6)$$

The different locations of the tunnel ring will have a different F_{S1} value due to the different M and N value. Therefore, the minimum value of F_{S1} is selected as the final F_{S1} result, which means the most dangerous situation along the tunnel ring is considered. The horizontal convergence of tunnel (ΔD_h) is commonly adopted to evaluate the factor of safety of tunnel serviceability (SLS), F_{S2}. According to the Chinese metro code [28], the maximum convergence deformation of tunnel must be controlled within 0.4–0.6% D (D means the outer diameter of tunnel). For conservative evaluation of tunnel serviceability, the 0.4%D is generally considered the limit value in this study. Therefore, the F_{S2} can be defined as:

$$F_{S2} = \frac{0.4\%D}{\Delta D_h} \tag{7}$$

Figure 10 shows the comparison for the F_{S1} value of tunnels under different borehole schemes. In total, the mean value of the F_{S1} getting closer and closer to the result of the BS8 borehole layout scheme. Since there are only eight boreholes, we can take the results of using eight boreholes as the "real" result. In other words, the simulated strata are closer to the "real" strata. Thus, the calculated mean value of the F_{S1} is closer to the "real" F_{S1}. It also means that the uncertainty of simulated strata is decreased with the increase in boreholes. As can be seen from the black line of Fig. 10, there is also a trendy that the COV decreases to 0 and the value of F_{S1} is closer and closer to the "real" F_{S1} with the increase in the boreholes. However, it is not a linear relationship which also indicates the weight of each borehole is different. For example, the results of the BS3A and BS3B layout scheme have a big difference which is caused by the different weights of borehole B5 and B3. The COV of the value of F_{S1} for BS4B layout scheme is less than BS5B and BS6 layout schemes. Comparing with the result of BS4A and BS4B, it can be found that the combination of borehole B4 and B6 is better than the combination of B3 and B5. Although these two combinations are located at both sides of the tunnel, the combination of B4 and B6 has a larger GUI value. In addition, when boreholes B3, B5 and B7 are together, it will cause the wrong simulation of the layer of soil type 4 between soil type 2 and soil type 3, as shown in Fig. 7. This is the reason that the result of borehole layout scheme BS5B *[boreholes (1,3,5,7,8)]* and BS6 *[boreholes (1,2,3,5,7,8)]* is not better than result of BS4B *[boreholes (1,4,6, 8)]*.

The results of factor of safety of tunnel serviceability for different borehole schemes are shown in Fig. 11. As introduced before, the outer diameter $D = 6.2$ m, so the limited horizontal deformation $0.4\%D$ is 24.8 mm. Thus,
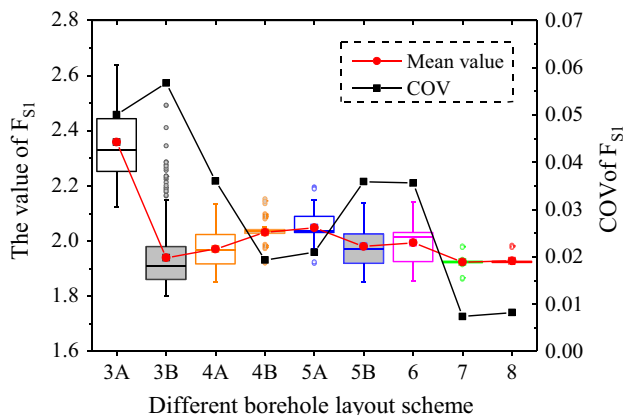
the F_{S2} value can be calculated using Eq. (7). For example, the "real" ΔD_h for the most likely realization for all eight boreholes is 15.759 mm. Therefore, the value of F_{S2} can be calculated as 24.8/15.759 = 1.574. As shown in Fig. 11, the distribution of F_{S2} of different layout schemes is relatively different. For example, the obtained value of F_{S2} for the BS3A layout scheme is overestimated, which is very dangerous in practical engineering. The histogram of BS4A *[boreholes (1,3,5,8)]*, BS5B *[boreholes (1,3,5,7,8)]* and BS6 *[boreholes (1,2,3,5,7,8)]* layout scheme is very similar, which means the boreholes B3 and B5 play a more significant role than B2 and B7. B3 and B5 boreholes not only have a larger GUI value, but they are also closer to the tunnel influence zone, so they have greater weight for evaluating the tunnel performance under uncertain strata. In summary, there is a nonlinear relationship between the response of tunnel structure and the number of boreholes indicating different boreholes have different weights. The boreholes with larger GUI values and near tunnel influence zones have a larger weight for estimating tunnel structural performance.

Figure 12 shows the relationship between the unrevealed GUI and the uncertainty of FS of tunnel. The unrevealed GUI value is the sum of the GUI of other boreholes not included in this borehole scheme. Taking the BS5B *[boreholes (1,3,5,7,8)]* as an example, the boreholes not included are boreholes 2, 4 and 6. As given in Table 5, the GUI value of boreholes 2, 4 and 6 is 26.7%, 45% and 33.3%, respectively. Thus, the unrevealed GUI value by BS5B borehole scheme is 1.05 (26.7% + 45% + 33.3% = 105%). The COV of FS of tunnel is used to evaluate the uncertainty of FS of tunnel in this section. There is a positive correlation between the unrevealed GUI and COV of FS of tunnel. It means that the greater the unrevealed uncertainty of the borehole scheme, the greater the uncertainty of the tunnel safety factor. This also illustrates the effectiveness of the proposed method for evaluating geological uncertainty.

5 Case study of Shanghai site

5.1 Borehole data of Shanghai

Figure 13 shows the geological profile revealed by boreholes of Huaxia middle road in Shanghai. Compared with the Norway site, the level of geological uncertainty of the selected Shanghai site is much lower which is determined by the historical reasons of the stratum formation. As shown in Fig. 13, there are six soil layers which are filled soil, silty clay, muddy silty clay, muddy clay, clay and silt. For clarity, they are named soil type 1 to 6 from up to down, respectively. The domain is a rectangular area with an x, z range of [0 m, 82 m] and [0 m, 50 m], respectively.
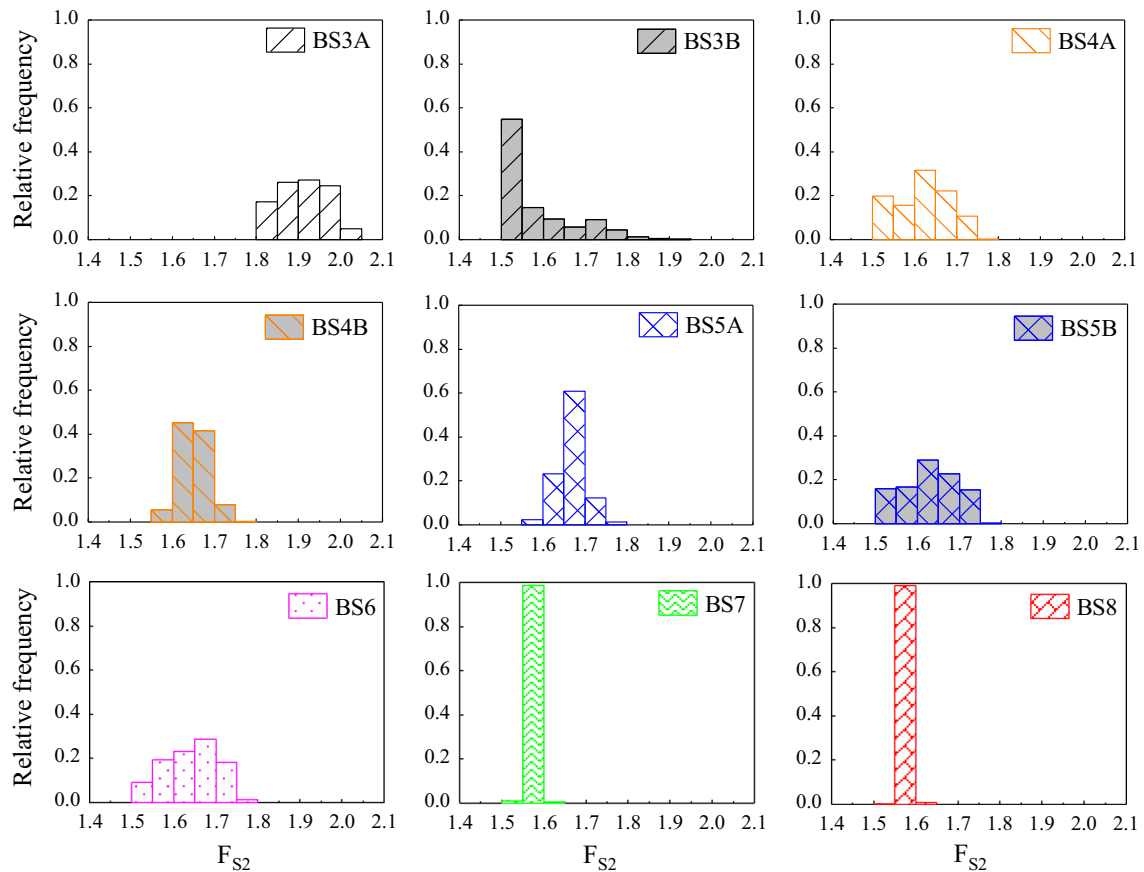

Fig. 10 F_{S1} of tunnel for different borehole schemes

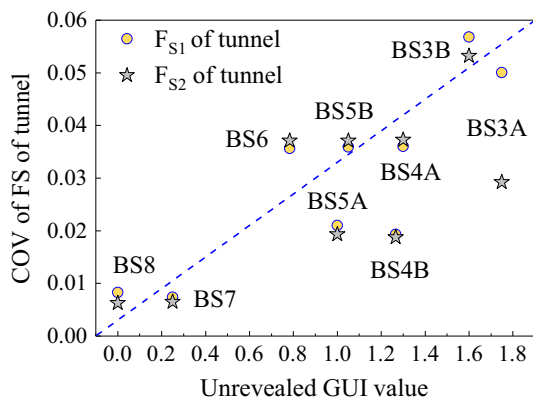**Fig. 11** F_{S2} of tunnel for different borehole schemes

Fig. 12 Relationship between the unrevealed GUI and the uncertainty of FS

5.2 Generating stratigraphic realizations

The VTPMs and HTPMs for various boreholes layout schemes of the collected Shanghai sites are presented in Tables 6 and 7. It can be seen that the difference in the VTPMs and HTPMs for different borehole layout schemes is very tiny. In other words, the effect of the borehole layout scheme is little on the stratum simulation.
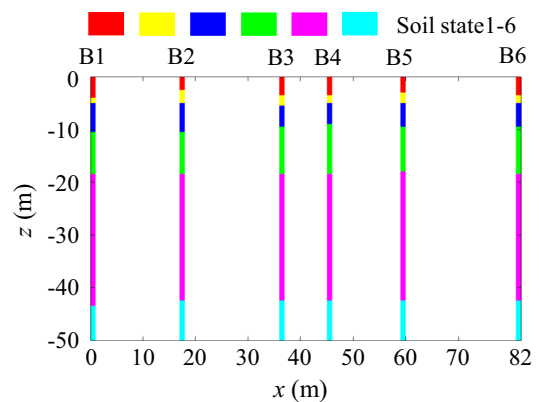

Fig. 13 Geological profile revealed by boreholes in Shanghai site

Meanwhile, the value on the diagonal of HTPMs for four borehole layout schemes is all larger than 0.99, which means the lithology is deposited in a very horizontal direction. It also indicates that the level of uncertainty in horizontal direction is low.

Figure 14 shows the most likely realization of different borehole layout schemes for the selected Shanghai site. The simulated results have a slight difference even if the different boreholes are used as the input of the CMC model.

Table 6 VTPMs for various layout schemes of Shanghai site

State	1	2	3	4	5	6	State	1	2	3	4	5	6
(a) BS3 [boreholes (1,3,6)]							*(b) BS4 [boreholes (1,2,5,8)]*						
1	0.864	0.136	0.000	0.000	0.000	0.000	1	0.846	0.154	0.000	0.000	0.000	0.000
2	0.000	0.667	0.333	0.000	0.000	0.000	2	0.000	0.714	0.286	0.000	0.000	0.000
3	0.000	0.000	0.893	0.107	0.000	0.000	3	0.000	0.000	0.900	0.100	0.000	0.000
4	0.000	0.000	0.000	0.942	0.058	0.000	4	0.000	0.000	0.000	0.940	0.060	0.000
5	0.000	0.000	0.000	0.000	0.979	0.021	5	0.000	0.000	0.000	0.000	0.979	0.021
6	0.000	0.000	0.000	0.000	0.000	1.000	6	0.000	0.000	0.000	0.000	0.000	1.000
(c) BS5 [boreholes (1,3,4,5,6)]							*(d) BS6 [boreholes (1,2,3,4,5,6)]*						
1	0.857	0.143	0.000	0.000	0.000	0.000	1	0.850	0.150	0.000	0.000	0.000	0.000
2	0.000	0.688	0.313	0.000	0.000	0.000	2	0.000	0.714	0.286	0.000	0.000	0.000
3	0.000	0.000	0.889	0.111	0.000	0.000	3	0.000	0.000	0.893	0.107	0.000	0.000
4	0.000	0.000	0.000	0.943	0.057	0.000	4	0.000	0.000	0.000	0.942	0.058	0.000
5	0.000	0.000	0.000	0.000	0.979	0.021	5	0.000	0.000	0.000	0.000	0.979	0.021
6	0.000	0.000	0.000	0.000	0.000	1.000	6	0.000	0.000	0.000	0.000	0.000	1.000

Table 7 HTPMs for various layout schemes of Shanghai site

State	1	2	3	4	5	6	State	1	2	3	4	5	6
(a) BS3 [boreholes (1,3,6), K = 100]							*(b) BS4 [boreholes (1,2,5,8), K = 85]*						
1	0.998	0.002	0.000	0.000	0.000	0.000	1	0.998	0.002	0.000	0.000	0.000	0.000
2	0.000	0.995	0.005	0.000	0.000	0.000	2	0.002	0.993	0.005	0.000	0.000	0.000
3	0.000	0.000	0.998	0.001	0.000	0.000	3	0.000	0.000	0.999	0.001	0.000	0.000
4	0.000	0.000	0.000	0.999	0.001	0.000	4	0.000	0.000	0.000	0.999	0.001	0.000
5	0.000	0.000	0.000	0.000	1.000	0.000	5	0.000	0.000	0.000	0.000	1.000	0.000
6	0.000	0.000	0.000	0.000	0.000	1.000	6	0.000	0.000	0.000	0.000	0.000	1.000
(c) BS5 [boreholes (1,3,4,5,6), K = 65]							*(d) BS6 [boreholes (1,2,3,4,5,6), K = 36]*						
1	0.997	0.003	0.000	0.000	0.000	0.000	1	0.995	0.005	0.000	0.000	0.000	0.000
2	0.001	0.992	0.007	0.000	0.000	0.000	2	0.005	0.984	0.011	0.000	0.000	0.000
3	0.000	0.000	0.998	0.002	0.000	0.000	3	0.000	0.001	0.996	0.003	0.000	0.000
4	0.000	0.000	0.000	0.999	0.001	0.000	4	0.000	0.000	0.000	0.998	0.002	0.000
5	0.000	0.000	0.000	0.000	1.000	0.000	5	0.000	0.000	0.000	0.000	0.999	0.001
6	0.000	0.000	0.000	0.000	0.000	1.000	6	0.000	0.000	0.000	0.000	0.000	1.000

The centre line of the tunnel in vertical and horizontal directions is located at 20 m and 41 m for all layout schemes. The parameters of all six soil layers are given in Table 8. The tunnel parameters are the same as those introduced in Sect. 4. It can be imagined that the tunnel structural performance does not differ much under the four borehole layout schemes.

5.3 Evaluation of borehole uncertainty of Shanghai site

Following the proposed approach, the GUI values of each borehole and the average level of the Shanghai site are presented in Table 9. The simulated depth of the Shanghai site is 50 m, and the total number of cells is 100 with 0.5-m sampling intervals. There are total collected six boreholes for this site. Similarly, the most likely simulated strata realization is adopted as the simulated result to compare with the virtual result to count the different number of cells for each borehole, as shown in Table 9. The virtual strata are obtained using the borehole B1 and B6 of the Shanghai site with the method introduced in Sect. 3. It can be seen that the GUI value is very small and the average level of GUI is only 2.5%. The GUI value is only about 7% which is much less than the uncertain level of the collected Norway site (34.2%). It indicates that the effect of geological uncertainty of collected Shanghai site on tunnel structural performance will be much less than Norway site.
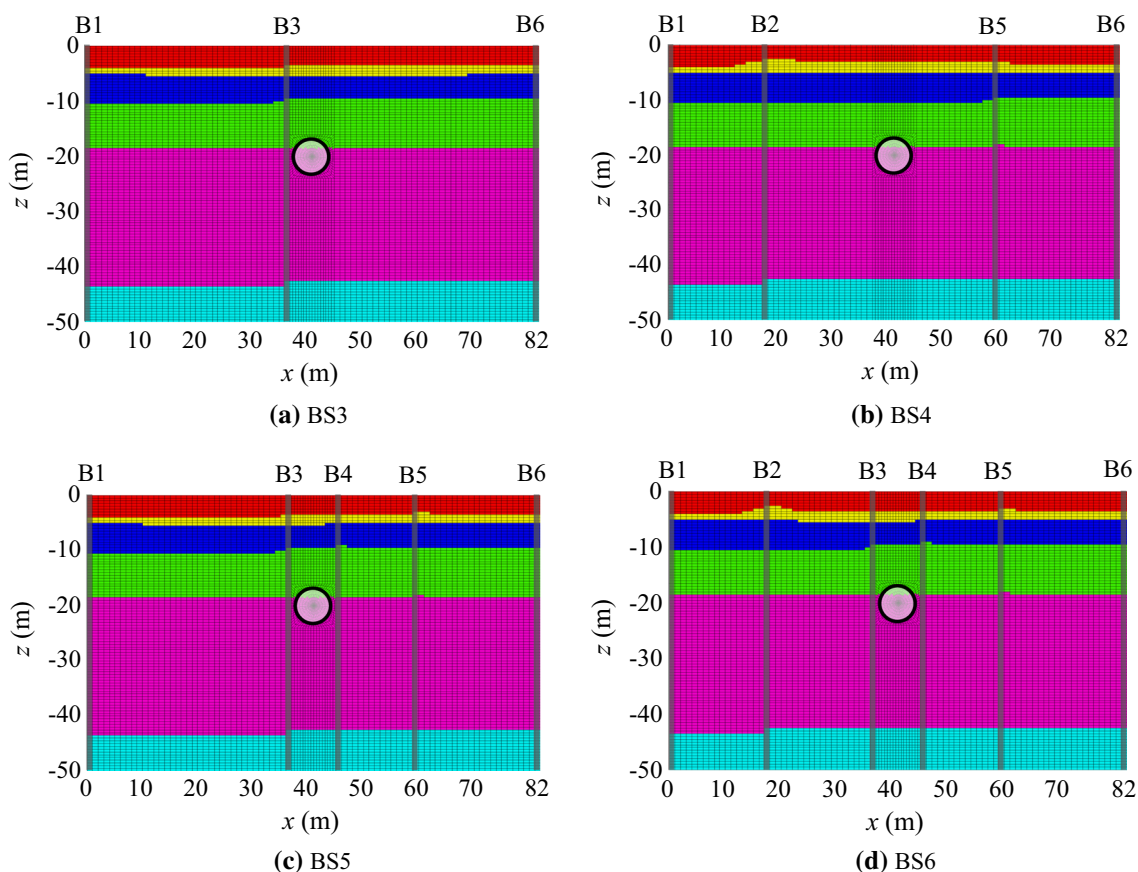
Fig. 14 Most likely realizations for different borehole schemes of Shanghai site

Table 8 Parameters for various types of Shanghai soil layer

Soil types	E (MPa)	v	c' (kPa)	φ' (°)	γ (kN/m³)
State 1	21.5	0.33	0	22	1800
State 2	41.5	0.29	10	27.5	1860
State 3	17.5	0.32	12	21	1770
State 4	11.5	0.35	14	12	1690
State 5	22.5	0.28	20	16.5	1800
State 6	70.5	0.26	1	35	1890

Table 9 Geological uncertainty index for Shanghai case

Borehole	B2	B3	B4	B5	Average
Different cells	4	3	1	2	2.5
GUI	4%	3%	1%	2%	2.5%

5.4 Results analysis

The comparison of box plot for different borehole schemes of Shanghai site is plotted in Fig. 15. It can be seen that the

results are very similar because the simulated strata do not have much difference. The "real" $\Delta D_h = 13.424$ mm which is the calculated tunnel structural response of the most likely realization using all six collected boreholes. The RE value of different borehole layout schemes is less than 1% which also means the level of geological uncertainty is relatively smaller. Meanwhile, the geological uncertainty has a little influence on the embedded tunnel in
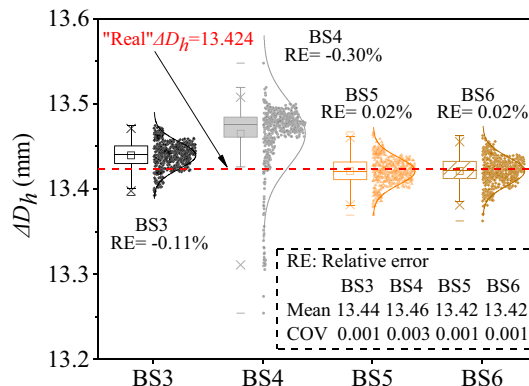

Fig. 15 Comparison of calculated result for different borehole schemes of Shanghai site

this site. However, there is an interesting thing that the RE value of the BS4 scheme *[boreholes (1,2,5,6)]* is actually greater than that of BS3 *[boreholes (1,3,6)]*. As given in Table 9, it can be known that the total GUI value of the BS4 layout scheme is 6% (4% + 2% = 6%) and that for the BS3 layout scheme is 3%. Meanwhile, the number of boreholes of the BS4 layout scheme is bigger than the BS3 layout scheme. However, it is worth mentioning that the borehole B3 is much nearer the tunnel than B2 and B5. This phenomenon confirms that the boreholes located near the tunnel also have a larger weight to affect the structural performance of tunnel, as discussed in Sect. 4. Through two case studies, it can be seen that the proposed GUI indicator can be used to quantitatively evaluate the uncertain level of each borehole and the average uncertain level of the entire site.

6 Conclusions

This paper investigates the effect of the borehole layout scheme on evaluating uncertainty in the factor of safety of tunnel structural performance caused by geological uncertainty. The improved coupled Markov chain conditioning on the borehole data of Norway and Shanghai sites are adopted to model the geological uncertainty. Based on the analysis result, the following conclusions are tentatively summarized.

(1) The proposed probabilistic analysis framework combines the geological uncertainty and simulated tunnel numerical model based on limited borehole data. The proposed mapping method can well map the simulated stratigraphic to the complex and irregular mesh of the numerical model. This method can also be applied to other geotechnical engineering problems.

(2) A GUI indicator was proposed to quantitatively evaluate the geological uncertainty. It can assess the level of uncertainty of each borehole and entire site. The borehole with a larger GUI value significantly influences the geological uncertainty of model strata. There is a positive correlation between the unrevealed GUI and the uncertainty of safety factor of tunnel, indicating the effectiveness of the proposed method for evaluating geological uncertainty.

(3) With the number of boreholes increasing, the safety factor of tunnel structural performance converges to the "real" answer and the COV generally decreases. Meanwhile, the boreholes with a larger GUI value and nearer the tunnel location have a greater weight to affect the embedded tunnel structural performance in uncertain geological strata.

References

1. Cao W, Zhou A, Shen SL (2021) An analytical method for estimating horizontal transition probability matrix of coupled Markov chain for simulating geological uncertainty. Comput Geotech. https://doi.org/10.1016/j.compgeo.2020.103871
2. Carle SF, Labolle EM, Weissmann GS, Van Brocklin D, Fogg GE (1998) Conditional simulation of hydrofacies architecture: a transition probability/Markov approach. Hydrogeol Models Sediment Aquifers Concepts Hydrogeol Environ Geol 1:147–170
3. Chen FY, Wang L, Zhang WG (2019) Reliability assessment on stability of tunnelling perpendicularly beneath an existing tunnel considering spatial variabilities of rock mass properties. Tunn Undergr Space Technol 88:276–289. https://doi.org/10.1016/j.tust.2019.03.013
4. Chiles JP, Delfiner P (1999) Geostatistics: modeling spatial uncertainty. Wiley, New York
5. Cross GR, Jain AK (1983) Markov random field texture models. IEEE Trans Pattern Anal Mach Intell 1:25–39
6. De Marsily G, Delay F, Gonçalvès J, Renard P, Teles V, Violette S (2005) Dealing with spatial heterogeneity. Hydrogeol J 13(1):161–183. https://doi.org/10.1007/s10040-004-0432-3
7. Deng ZP, Li DQ, Qi XH, Cao ZJ, Phoon KK (2017) Reliability evaluation of slope considering geological uncertainty and inherent variability of soil parameters. Comput Geotech 92:121–131. https://doi.org/10.1016/j.compgeo.2017.07.020
8. Elfeki A, Dekking M (2001) A Markov chain model for subsurface characterization: theory and applications. Math Geol 33(5):569–589. https://doi.org/10.1023/A:1011044812133
9. Elfeki AMM, Dekking FM (2005) Modelling subsurface heterogeneity by coupled Markov chains: directional dependency, Walther's law and entropy. Geotech Geol Eng 23(6):721–756. https://doi.org/10.1007/s10706-004-2899-z
10. Elkateb T, Chalaturnyk R, Robertson PK (2003) An overview of soil heterogeneity: quantification and implications on geotechnical field problems. Can Geotech J 40(1):1–15. https://doi.org/10.1139/t02-090
11. Gong WP, Juang CH, Ii JRM, Tang HM, Wang QQ, Huang HW (2018) Probabilistic analysis of tunnel longitudinal performance based upon conditional random field simulation of soil properties. Tunn Undergr Space Technol 73:1–14. https://doi.org/10.1016/j.tust.2017.11.026
12. Gong WP, Tang HM, Wang H, Wang XR, Juang CH (2019) Probabilistic analysis and design of stabilizing piles in slope considering stratigraphic uncertainty. Eng Geol 259:105162. https://doi.org/10.1016/j.enggeo.2019.105162
13. Gong WP, Wang L, Juang CH, Zhang J, Huang HW (2014) Robust geotechnical design of shield-driven tunnels. Comput Geotech 56(1):191–201. https://doi.org/10.1016/j.compgeo.2013.12.006
14. Hu QF (2006) Risk analysis and its application for tunnel works based on research of stratum and soil spatial variability. Ph.D. Dissertation, Shanghai: Tongji University
15. Huang H, Xu L, Yan JL, Yu ZK (2006) Study on transverse effective rigidity ratio of shield tunnels. Chin J Geotech Eng 28(1):11–18

16. Huang HW, Shao H, Zhang DM, Wang F (2017) Deformational responses of operated shield tunnel to extreme surcharge: a case study. Struct Infrastruct Eng 13(3):345–360. https://doi.org/10.1080/15732479.2016.1170156

17. Huang HW, Xiao L, Zhang DM, Zhang J (2017) Influence of spatial variability of soil Young's modulus on tunnel convergence in soft soils. Eng Geol 228:357–370. https://doi.org/10.1016/j.enggeo.2017.09.011

18. Huang HW, Zhang DM (2016) Resilience analysis of shield tunnel lining under extreme surcharge: characterization and field application. Tunn Undergr Space Technol 51:301–312

19. Itasca (2016) FLAC, fast Lagrangian analysis of continua: User's guide, version 8.0. Minneapolis: Itasca.

20. Jin DL, Shen ZC, Yuan DJ (2020) Effect of spatial variability on disc cutters failure during TBM tunneling in hard rock. Rock Mech Rock Eng. https://doi.org/10.1007/s00603-020-02192-2

21. Kawa M, Puła W (2020) 3D bearing capacity probabilistic analyses of footings on spatially variable c–φ soil. Acta Geotech 15(6):1453–1466. https://doi.org/10.1007/s11440-019-00853-3

22. Kulhawy FH, Mayne PW (1990) Manual on estimating soil properties for foundation design. Electric Power Research Institute, Washington

23. Li DQ, Qi XH, Cao ZJ, Tang XS, Phoon KK, Zhou CB (2016) Evaluating slope stability uncertainty using coupled Markov chain. Comput Geotech 73:72–82. https://doi.org/10.1016/j.compgeo.2015.11.021

24. Li JH, Cai YM, Li XY, Zhang LM (2019) Simulating realistic geological stratigraphy using direction-dependent coupled Markov chain model. Comput Geotech 115:103147. https://doi.org/10.1016/j.compgeo.2019.103147

25. Li Z, Wang XR, Wang H, Liang RY (2016) Quantifying stratigraphic uncertainties by stochastic simulation techniques based on Markov random field. Eng Geol 201(2016):106–122. https://doi.org/10.1016/j.enggeo.2015.12.017

26. Lloret-Cabot M, Fenton GA, Hicks MA (2014) On the estimation of scale of fluctuation in geostatistics. Georisk Assess Manag Risk Eng Syst Geohazards 8(2):129–140. https://doi.org/10.1080/17499518.2013.871189

27. Matheron G, Beucher H, De Fouquet C, Galli A, Guerillot D, Ravenne C (1987) Conditional simulation of the geometry of fluvio-deltaic reservoirs. In: Spe annual technical conference and exhibition. Society of Petroleum Engineers

28. Ministry of Construction of the People's Republic of China (2003) Code for design of metro. China Building Industry Press, Beijing

29. Mollon G, Dias D, Soubra AH (2013) Probabilistic analyses of tunneling-induced ground movements. Acta Geotech 8(2):181–199. https://doi.org/10.1007/s11440-012-0182-7

30. Mylius A (2007) Sao Paulo collapse: NATM used despite failure history. New Civil Engineer International

31. Pan QJ, Dias D (2017) Probabilistic evaluation of tunnel face stability in spatially random soils using sparse polynomial chaos expansion with global sensitivity analysis. Acta Geotech 12(6):1415–1429. https://doi.org/10.1007/s11440-017-0541-5

32. Pan YT, Yao K, Phoon KK, Lee FH (2019) Analysis of tunnelling through spatially-variable improved surrounding—a simplified approach. Tunn Undergr Space Technol 93:103102. https://doi.org/10.1016/j.tust.2019.103102

33. Phoon KK, Kulhawy FH (1999) Characterization of geotechnical variability. Can Geotech J 36(4):612–624. https://doi.org/10.1139/t99-038

34. Qi XH, Li DQ, Phoon KK, Cao ZJ, Tang XS (2016) Simulation of geologic uncertainty using coupled Markov chain. Eng Geol 207:129–140. https://doi.org/10.1016/j.enggeo.2016.04.017

35. Strebelle S (2002) Conditional simulation of complex geological structures using multiple-point statistics. Math Geol 34(1):1–21. https://doi.org/10.1023/A:1014009426274

36. Wang F, Shi JK, Huang HW, Zhang DM, Liu DJ (2020) A horizontal convergence monitoring method based on wireless tilt sensors for shield tunnels with straight joints. Struct Infrastruct Eng. https://doi.org/10.1080/15732479.2020.1801767

37. Wang H, Wellmann JF, Li Z, Wang XR, Liang RY (2017) A segmentation approach for stochastic geological modeling using hidden Markov random fields. Math Geosci 49(2):145–177. https://doi.org/10.1007/s11004-016-9663-9

38. Wang L, Wu CZ, Gu X, Liu HL, Mei GX, Zhang WG (2020) Probabilistic stability analysis of earth dam slope under transient seepage using multivariate adaptive regression splines. Bull Eng Geol Environ 79(6):2763–2775. https://doi.org/10.1007/s10064-020-01730-0

39. Wang XR (2020) Uncertainty quantification and reduction in the characterization of subsurface stratigraphy using limited geotechnical investigation data. Undergr Space 5(2):125–143. https://doi.org/10.1016/j.undsp.2018.10.008

40. Wang XR, Li Z, Wang H, Rong QG, Liang RY (2016) Probabilistic analysis of shield-driven tunnel in multiple strata considering stratigraphic uncertainty. Struct Saf 62:88–100. https://doi.org/10.1016/j.strusafe.2016.06.007

41. Wang XR, Wang H, Liang RY (2018) A method for slope stability analysis considering subsurface stratigraphic uncertainty. Landslides 15(5):925–936. https://doi.org/10.1007/s10346-017-0925-5

42. Wang XR, Wang H, Liang RY, Zhu HH, Di HG (2018) A hidden Markov random field model based approach for probabilistic site characterization using multiple cone penetration test data. Struct Saf 70:128–138. https://doi.org/10.1016/j.strusafe.2017.10.011

43. Working Group No ITA (2000) Guidelines for the design of shield tunnel lining. Tunn Undergr Space Technol 15(3):303–331. https://doi.org/10.1016/S0886-7798(00)00058-4

44. Zhang DM, Huang HW, Hu QF, Jiang F (2015) Influence of multi-layered soil formation on shield tunnel lining behavior. Tunn Undergr Space Technol 47:123–135. https://doi.org/10.1016/j.tust.2014.12.011

45. Zhang DM, Liu ZS, Wang RL, Zhang DM (2019) Influence of grouting on rehabilitation of an over-deformed operating shield tunnel lining in soft clay. Acta Geotech 14(4):1227–1247. https://doi.org/10.1007/s11440-018-0696-8

46. Zhang DM, Zhang JZ, Huang HW, Qi CC, Chang CY (2020) Machine learning-based prediction of soil compression modulus with application of 1D settlement. J Zhejiang Univ A Sci 21(6):430–444. https://doi.org/10.1631/jzus.A1900515

47. Zhang JZ, Huang HW, Zhang DM, Zhou ML, Tang C, Liu DJ (2021) Effect of ground surface surcharge on deformational performance of tunnel in spatially variable soil. Comput Geotech 136:104229. https://doi.org/10.1016/j.compgeo.2021.104229

48. Zhang WG, Han L, Gu X, Wang L, Chen FY, Liu HL (2020) Tunneling and deep excavations in spatially variable soil and rock masses: a short review. Undergr Space. https://doi.org/10.1016/j.undsp.2020.03.003

49. Zhao S, Zhang DM, Huang HW (2020) Deep learning–based image instance segmentation for moisture marks of shield tunnel lining. Tunn Undergr Space Technol 95:103156. https://doi.org/10.1016/j.tust.2019.103156